Laboratory, Field, and Modeling Studies of CO_2 Hydrate Composite Particles Formed by Direct Injection of CO_2 in the Ocean

Costas Tsouris[1] (tsourisc@ornl.gov), Liyuan Liang[1] (liangl@ornl.gov), David Riestenberg[1] (riestenbergd@ornl.gov), Olivia West[1] (westor@ornl.gov), Sangyong Lee[1] (kfsl003@tamuk.edu), Jorge Gabitto[1], Peter Brewer[2] (brpe@mbari.org), Ed Peltzer[2] (etp3@mbari.org), Eric Adams[3] (eeadams@mit.edu)

[1]Oak Ridge National Laboratory, Oak Ridge, TN, 37831
[2]Monterey Bay Aquarium Research Institute, Moss Landing, CA, 95039
[3]Massachusetts Institute of Technology, Cambridge, MA, 02139

Abstract

Partial conversion of CO_2 to CO_2 hydrate in seawater creates a negatively buoyant composite at intermediate ocean depths. This paper describes laboratory experiments in which seawater and liquid CO_2 were premixed to produce a liquid CO_2/water/CO_2 hydrate composite (referred to as CO_2 hydrate composite, or simply composite, hereafter) using a co-flow jet reactor in a 70-L pressurized vessel. CO_2 hydrate is a nonstoichiometric solid phase of CO_2 and water that is thermodynamically stable at pressures equivalent to depths >500 m at ~ 4 °C (*1*). Pure hydrate is approximately 10% denser than seawater (*2*). Therefore, complete conversion of liquid CO_2 to form pure CO_2 hydrate would produce sinking particles at relatively shallow depths. Complete conversion of CO_2 to the hydrate phase, however, would be a slow, energy intensive process. It can be shown however, that complete conversion is not necessary to create negatively buoyant CO_2 particles. The bulk density of CO_2 hydrate composite is given by (*3*):

$$\rho_{com} = \frac{1 + n(18/44)x_h}{(1-x_h)/\rho_c + (1+n(18/44))x_h/\rho_h} \quad (1)$$

where n is the hydration number, x_h is the mole fraction of CO_2 converted into hydrate, and ρ_c is the density of CO_2. Using n = 7 (*3*) and a corresponding density of ρ_h = 1100 kg/m^3 *(2,3)*, a CO_2 hydrate composite mass density will be greater than the ambient seawater at 1500, 1300, and 1100 m if the mole fraction of CO_2 converted to hydrate were at least 0.19, 0.22 and 0.24, respectively. Thus, only moderate amounts of CO_2 hydrate are needed to produce a sinking composite at intermediate ocean depths (1000 – 1500 m).

Using the concept of premixing seawater into a liquid CO_2 stream, we produced a negatively buoyant composite material at conditions simulating intermediate ocean depths (~1000–1300 m) at Oak Ridge National Laboratory (ORNL) (*4*). Recently, this system was successfully tested in ocean water depths of 1100 – 1300 m at Monterey Bay, California, in collaboration with the Monterey Bay Aquarium Research Institute (MBARI). Such a development is significant because releasing CO_2 in a form that will sink through the water column will prolong its residence time in the ocean. This approach allows efficient CO_2 injections at a lower operating cost when compared with producing dense liquid CO_2 at depths greater than 3000 m. Additionally, scaling up the proposed injector design can potentially produce large masses of CO_2 hydrate composite with low surface-to-volume ratio, resulting in increased settling velocities and slower dissolution rates when compared to small hydrate particles, such as those made in stirred tank reactors (*5*). Increased settling velocity and potentially reduced dissolution rates will increase the dispersion of CO_2 in the ocean, improve sequestration efficiency, and reduce negative impacts on the marine environment.

Models and computer codes simulating the hydrodynamics and dissolution of a hydrate composite particle plume have been developed at Massachusetts Institute of Technology (MIT). It has been shown that because dissolution of CO_2 particles produces a denser solution than the surrounding seawater, the plume sinks with time.

Description

Laboratory Developments

An injector system was developed to study the conversion of liquid CO_2 to CO_2 hydrate and produce a negatively buoyant CO_2 hydrate composite (Figure 1). To promote hydrate formation with a continuous CO_2 feed a co-flow injector was designed by entraining water into a stream of CO_2. The injector consists of an outer tube and a concentrically located inner capillary tube (0.127×10^{-3}-m ID) for liquid CO_2 and water, respectively. The capillary tube terminates approximately 0.14 m from the end of the outer tube, creating a zone in which the liquid CO_2 and water can mix before being discharged into the ambient water. The injector was tested using a 70-L temperature-controlled, high-pressure seafloor process simulator (SPS) that simulates conditions at ocean depths up to 2000 m (*6*).

In a typical experiment, the SPS was filled with water, pressurized to near experimental levels (10 to 13 MPa), and then cooled in a temperature-controlled (cold) room to the experimental temperature (4–5ºC). Liquid CO_2 and water, pre-cooled to the experimental temperature, were delivered using syringe pumps through the injector into the SPS at predetermined flowrates of 15–25 and 2–10 ml/min, respectively. The material ensuing from the injector was observed and recorded by a video camera through one of the sapphire windows of the SPS. By introducing water into CO_2 through the co-flow injector, a semi solid-like material was extruded from the injector (Figure 1). Close observation with a borescope system showed hydrate-covered water droplets of uniform size "fused" together (Figure 2). The average drop diameter was found to be ~270 μm with a standard deviation of ~80 μm. Several sets of injection experiments were conducted at ~4 ºC and at 10.3, 11.7, and 13.1 MPa. Depending on the pressure, temperature, and flowrate conditions, the hydrate composite may be positively buoyant (Figure 3a) or negatively buoyant (Figure 3b). The main difference between the experimental conditions used in Figures 3a and 3b is the flowrate of water and CO_2.

Figure 4 shows the measured maximum volumetric flowrate of CO_2 at a given water flowrate that was necessary to form a negatively buoyant hydrate composite. When the maximum CO_2 flowrate is exceeded, a positively buoyant composite is obtained. With a CO_2 flowrate equal to or lower than the maximum, a negatively buoyant composite is produced. The positively buoyant regime corresponds to the region above the line for the thermodynamic conditions represented by each line, while the negatively buoyant regime falls below the line. For instance, if the initial flow conditions fall in the positively buoyant regime (point A in Figure 4), one can decrease the CO_2 flowrate (point B) or increase the water flowrate (point C) to switch to the negative buoyancy regime, provided that the other conditions remained unchanged. When the operating conditions are changed from point A to B or C, the hydrate composite becomes denser than the surrounding water. The minimum conversion of CO_2 required to produce a denser composite has been shown to be intrinsic to pressure and temperature and independent of the water and CO_2 flowrate. However, it was determined experimentally that at a given CO_2 flowrate, there is a minimum water injection rate that is necessary to make a denser composite product. This observation suggests that the water flowrate affects mixing and mass transport rates, which control the conversion of liquid CO_2 to hydrate in the reactor.

Field Testing of Injector

The coflow jet reactor was field tested in ocean waters from 1.1 to 1.3 km depth in Monterey Bay, California. The remotely operated vehicle (ROV) *Ventana* was deployed by the RV *Point Lobos* to perform the injections. The injector was placed in a Plexiglas box that was open at the top and bottom (Figure 5). This box allowed the injected composite particles to rise or fall freely based on their buoyancy but restricted lateral motion. Carbon dioxide and water were pumped via a piston assembly, as described earlier (*7*). Volumetric flow meters were used to measure the flowrates of the fluids as they were introduced into the coflow jet reactor. Injections were performed using a 1:1 ratio (run 163) of CO_2 to water at ~1000-m depth in order to produce a floating composite and with a 1:5 ratio at ~1300-m depth

(run 164) in order to produce a sinking composite. The size and velocity of the resultant particles were determined by using the ROV, which traveled vertically to follow a randomly selected particle through the water column and filmed the particle using a high-resolution camera (*7*). The composite particles appeared to be similar to those produced in laboratory experiments (Figure 3). Selected video frames in which the particle appeared to be oriented parallel to the front Plexiglas plane were used to determine the dimensions of the particle. Through these data, a composite velocity and density could be determined. From the density and size data, the composite fractional composition and dissolution rate were calculated (Table 1).

The vertical paths of three particles that were followed by the ROV are plotted in Figure 6. The particle from Run 163 (using a 1:1 flowrate ratio of CO_2:seawater) was observed to be positively buoyant, while two particles from Run 164 (using a 1:5 ratio) were observed to be neutrally buoyant. The masses of each component of the composite were converted to a mass fraction of the total particle mass. The mass fractions of liquid CO_2 and CO_2 hydrate were higher in the Run-163 than in Run-164 since the flowrate of CO_2 in the injector was the same as that of water. In all three injections, the densities of the composite particles (ρ_p) were very similar to that of the surrounding seawater (ρ_w). The values of the minimum CO_2 conversion (x_{h_min}) necessary to produce a neutrally buoyant particle were also very similar (calculated using eq 1 and $\rho_{com} = \rho_w$), providing an explanation for their low float/sink velocities.

The rate of particle shrinkage over time allows a comparison of the dissolution rates of composite particles with those observed for hydrate-covered CO_2 droplets by others. The overall particle shrinkage rates calculated for the injection runs 164_1226 and 164_1232 were 10.5×10^{-6} and 8.5×10^{-6} m/s, respectively, while that for injection run 163_1107 was 8.6×10^{-6} m/s. Brewer et al. (*7*) recently performed injections of CO_2 droplets at 800-m depth in Monterey Bay and reported a dissolution rate of approximately 3×10^{-6} m/s. The composite particles investigated in this work appear to have a higher shrinkage rate than those observed for droplets covered with hydrate, possibly owing to their porous and rough surface, as well as their higher interfacial surface area. Because the composite particles contain considerable amounts of water, it is reasonable to correct for the presence of water in order to convert the shrinkage rate to an equivalent CO_2 dissolution rate. If it is assumed that the CO_2 fraction is less than 1/3 of the initial mixture, then the dissolution rate corresponding to pure CO_2 averaged between 3×10^{-6} m/s and 3.5×10^{-6} m/s, which is similar to the values reported by Brewer and coworkers (*7*).

Due to pump limitations, the maximum water flowrate available for the SPS laboratory injections was ≤ 25 mL/min and in the ocean injections was limited to 50 mL/min, a direct comparison cannot be made between the water and CO_2 flow rates for creation of a sinking composite. However, if the laboratory results (Figure 4) were extrapolated to higher water flowrates, the maximum flowrate of CO_2 that will produce a sinking composite with 50 mL/min water would be 17.2 mL/min at 10.3 MPa and 28.4 mL/min at 13.1 MPa. Injection run 163_1107 was performed at 10.99 MPa with a CO_2 flowrate of 50 mL/min and produced a floating particle composite as predicted by the laboratory flowrate ratios. Injection runs 164_1226 and 164_1232, however, were performed with a CO_2 flowrate of 10 mL/min, which, according to the laboratory experiment, should give a negatively buoyant composite. Instead, the particles were neutrally buoyant. This result suggests a non-linear behavior, which should be expected because of the complexity of the system and the dependency on mixing conditions, e.g., saltwater vs freshwater. In terms of the capillary Reynolds number, in the laboratory experiments, N_{Re} varied between 2200 and 2900, which is close to the transitional region from laminar to turbulent flow. In the field injections, however, N_{Re} was approximately 5900, which is in the turbulent regime.

Plume Modeling (MIT)

An integral double plume model was developed to simulate the fate of negatively buoyant single and multi-phase discharges into the ocean (*8,9*). While the main focus is the discharge of hydrate composites, as described above, the model can also be applied to other negatively buoyant forms of CO_2 including dry ice (*10*), very cold liquid CO_2 (*11*), dense $CaCO_3$ slurries (*12*) or emulsions (*13*), or highly concentrated CO_2 and seawater solutions (*14-16*).

The model is a modification of the integral double plume model applied to positively buoyant plumes and calibrated to laboratory data for both positively and negatively buoyant discharges (*17,8*). Here the dispersed phase (e.g., solid CO_2 hydrates) and associated entrained water are modeled as a sinking inner plume, while the counter flowing intrusions created from peeling events are modeled as an outer plume. Plume evolution is described by entrainment fluxes of water, momentum, salt, heat and dissolved CO_2 from the ambient to the outer plume, from the outer to the inner plume and vice versa, and detrainment from the inner plume as indicated in Figure 7.

A sub-model controls the dissolution of CO_2 from the dispersed phase, which becomes a source of dissolved CO_2 for the inner model. For modeling liquid CO_2 droplets:

$$\frac{dM_c}{dt} = -AKC_s \tag{2}$$

where M_c is the mass of CO_2 in the droplet, A is its surface area, K is a mass transfer coefficient that depends on the droplet size and velocity (*18*) and C_s is the surface concentration which equals the solubility of CO_2 in the ocean. In modeling the behavior of liquid CO_2 droplets coated with a thin hydrate shell, Crounse et al. (*17*) modified Eqn. 6 using an inhibition factor λ:

$$\frac{dM_c}{dt} = -\lambda AKC_s \tag{3}$$

λ accounts for uncertainty in C_s associated with the hydrate shell; from Hirai et al. (*19*), $\lambda \cong 0.5$. The mass transfer model is further modified to apply to solid hydrates particles:

$$\frac{dM_h}{dt} = -\lambda AKC_s \frac{MW_{hyd}}{MW_{CO_2}} = -\Lambda AKC_s \tag{4}$$

Eqn. (4) differs from Eqn. (3) by the ratio of the molecular weights of CO_2 hydrate and pure CO_2 (152/44 $\cong$ 3.5) to account for the fact that every molecule of dissolving CO_2 yields an associated loss of water as well. Calibration of the model to the rate of solid hydrate shrinkage observed in the field by Rehder et al. (*20*), suggests $\Lambda = \lambda(MW_{hyd}/MW_{CO_2})$ should be in the range of 0.5 to 1.0. Somewhat higher values would be expected to apply to composites of liquid CO_2, solid hydrate and seawater.

An additional model modification allows simulation of multiple size fractions. Simulations comparing plume properties using a mono-dispersed size distribution, with those using poly-dispersed distributions (uniform, logarithmic and semi-logarithmic) having similar mean particle size showed little difference, suggesting that use of a single particle size is adequate (*8*).

In order to extend results beyond the near field influence of the plume, a simple relative diffusion model has been included. Horizontal, scale-dependent diffusivity is simulated based on data from Okubo (*21*), while vertical diffusion is ignored.

We have performed a number of sensitivity studies. Those described here entail discharge at a depth of 800 m in a stratification profile measured at Station Aloha north of Oahu and characterized by a stratification frequency $N = [(g/\rho)(d\rho/dz)]^{0.5}$ of 0.003 per second. To get a broad indication of the behavior of CO_2 hydrate releases, the mass injection rate of CO_2 was varied from 3.5 to 3500 kg/s, corresponding to pure CO_2 rates of 1 to 1000 kg/s. (130 kg/s is the approximate CO_2 mass rate for a 500 MW coal plant.) Initial particle diameter was varied between 0.5 and 5.0 cm.

Figure 8 shows sensitivity of maximum plume and average intrusion depths to particle diameter and mass flux. The plume group effect, indicated by the difference between the falling particle depth and the plume depth, increases modestly with particle diameter and markedly with mass flux. Plume depth itself increases strongly with particle diameter, as well as with mass flux. Average intrusion depth, an indicator

of sequestration efficiency, follows similar trends. The average intrusion depths are favorable in that they result in CO_2 trapping far below the release.

Figure 9 shows the modeled averaged excess dissolved inorganic carbon (DIC) and pH within the intrusion layer. Excess DIC concentration, which is inversely proportional to dilution (ratio of entrained seawater volume to volume of CO_2 discharge), decreases strongly with diameter and increases with mass injection rate. Although larger mass injection rates get lower dilution, they still produce considerable entrainment. For example, increasing mass flux by a factor of 1000 only increases DIC concentrations by a factor of about 4, implying an increase in volume flux of a factor of 250. The predicted average pH values follow a similar trend as DIC with the three lowest mass rates yielding predicted pH drops of less than one unit for diameters greater than about 2 cm.

Figure 10 shows excess DIC concentration and pH changes 1000 m downstream from release. In general, higher mass flux produces significantly less far field dilution because more volume is required to dilute the initially large concentration fields. For example, all of the far field DIC values for the 10 kg/s release are less than 3% of their near field values, whereas the far field concentrations for the 1000 kg/s runs exceed 20% of their near field values. This indicates a trade-off between the high near field mixing and deep penetration depths of large mass injection rates and the corresponding lower far field mixing.

Additional analyses were performed. Sensitivity to mass transfer was studied by varying Λ from 0.5 to 1. For 2-cm particles and a mass release rate of 10 kg/s, the maximum plume depth decreased by 1000 m and the pH drop increased by 0.5 units, highlighting the importance of having good mass transfer data. The effect of an ambient current (which is not explicitly included in our model) was considered using correlations from our lab experiments (*22*) that compare the predicted trap depth, h_T, for a plume in quiescent stratification, with the separation depth, h_S, of particles leaving a plume in an unstratified cross flow. Defining a current's effect to be weak/strong, if the ratio of h_T/h_S was less/greater than one, all plumes created with a CO_2 flux of 1 kg/s were strongly affected by a 5 cm/s current; plumes with a 10 kg/s flux were affected only for large particle diameters, while plumes with 100 to 1000 kg/s fluxes were not strongly affected. This trend is convenient since plumes that benefit most from the plume group effect are least sensitive to ambient current. Finally, a theoretical comparison was made between negatively buoyant hydrate plumes and "equivalent" positively buoyant droplet plumes, assuming a constant volumetric injection of 10 liters/s, similar mass transfer, and linear stratification. For particle/droplet diameters of 2.5 cm, the negatively buoyant plume fell about 20% further than the positively buoyant plume rose, while for diameters of 0.5 cm, the percentage increased to 91%. Greater sinking means both longer sequestration and greater mixing, highlighting the fluid mechanical advantage of having both dispersed and dissolved phase buoyancies acting in the same direction.

While the above results apply to pure hydrates, we have also simulated the fate of composites with composition similar to those produced in the lab (SPS) and at sea. Because individual composite particles were close to neutrally buoyant, they did not sink (or rise) very much, leading one to the initial conclusion that, without a greater hydrate conversion rate, the CO_2 would not sink. However, in a real application a stream of particles would be injected, and their dissolution would drive a local increase in seawater density creating a negatively buoyant plume that *would* sink significantly.

In Table 2, we calculate the sinking depth of a negatively buoyant plume formed from the dissolution of *neutrally* buoyant composite particles into ambient waters characterized by $N = 0.003\ s^{-1}$. Calculations are made for CO_2 mass injections of 1, 10, 100 and 1000 kg/s. The table also includes the corresponding average intrusion depths to which a plume of pure solid hydrates (i.e., 100 % conversion efficiency) would sink, and the average intrusion heights to which a droplet plume of pure liquid CO_2 (i.e., 0% conversion efficiency) would rise (or, in the case of large loadings, the slight depth to which such a plume would sink). Clearly a conversion rate of order 25 %, as reported herein, takes us a significant way towards maximum theoretical sinking.

Summary

In summary, a novel injector has been developed for the conversion of liquid CO_2 to CO_2 hydrate, with the objective to produce sinking particles in the ocean. The major advantage this injector offers is that it produces sinking plumes and therefore longer sequestration with injection only at intermediate ocean depths. This approach is less energy demanding than injecting CO_2 at depths greater than 3000 m. The injector was successfully tested in the laboratory and in the ocean.

Based on experimental data, we have demonstrated through plume simulations the advantages of the proposed injection method in terms of sequestration and dispersion of CO_2 in the ocean. However, more work is still needed in order to better understand and maximize the conversion of liquid CO_2 to CO_2 hydrate and enhance the advantages of the method.

References Cited

1) Brewer, P. G.; Friederich, G.; Peltzer, E. T.; Orr, F. M., Jr. *Science* **1999**, *284*, 943–945.
2) Liro,; C. R., Adams, E. E., Herzog, H. G. *Energy Convers. Manage.* **1992**, 33, 667–674.
3) Holder, G. D.; Cugini, A. V.; Warzinski, R. P. *Environ. Sci. Technol*. **1995**, *28*, 276–278.
4) West, O.; Tsouris, C.; Liang, L.; Lee, S.-Y.; McCallum, S. *AIChE J.*, **2003**, *49*, 283 – 285.
5) Yamasaki, A.; Wakatsuki, M.; Teng, H.; Yanagisawa, Y.; Ymada, K. *Energy* **2000**, 25, 85–96.
6) Phelps, T. J.; Peters, D. J.; Marshall, S. L.; West, O. R.; Liang, L.; Blencoe, J. G.; Alexiades, V.; Jacobs, G. K.; Naney, M. T.; Heck, J. L., Jr. *Rev. Sci. Instrum*. **2001**, 72, 1514–1521.
7) Brewer, P. G.; Peltzer, E. T.; Friederich, G.; Rehder, G. *Envir. Sci. Technol*., **2002**, 36, 5441-5446.
8) Wannamaker, E. J., "Modeling carbon dioxide hydrate particle releases in the deep ocean" MS thesis, **2002**, Dept of Civil & Environmental Engineering, MIT. Cambridge, MA.
9) Wannamaker, E.J.; Adams, E.E. **2003**, *in preparation.*
10) Nakashiki, N.; Ohsumi, T.; Shitashima, K. *Technical Report*, **1994**, Central Research Institute of Electric Power Industry, Abiko-City, Japan.
11) Aya, I.; Yamane, K.; Shiozaki, K. *Proc. GHGT-4 Conference* **1999**, 269-274.
12) Caldeira, K.; Rau, G.H. *Geophys.l Res. Lett.,* **2000**, 27(2): 225-228.
13) Golomb, D. *Proc. GHGT-6 Conference*. **2002**.
14) Haugan, P.; Drange, H. *Nature* **1992**, 357(28): 1065-1072.
15) Adams, E.E.; Golomb, D.; Zhang, X.Y.; Herzog, H.J. "Confined release of CO_2 into shallow sea water", in *Direct Ocean Disposal of Carbon Dioxide*" **1995**, TERRAPUB, Tokyo, 153-164.
16) Saito, T.; Kajishima, T.; Naguosa, R. *Envir. Sci. Technol.* **2000**, *34*, 4140-4145.
17) Crounse, B.C.; Adams, E.E.; Socolofsky, S.A.; Harrison, T.H. *Proc. GHGT-5 Conference* **2001**, 411-416.
18) Clift, R.; Grace, J.R.; Weber, M.E. *Bubbles, Drops and Particles*; **1978**, Academic Press; New York.
19) Hirai, S.; Okazaki, K.; Tabe, Y.; Hijikata, K; Mori, Y. *Energy* **1997**, *22(2/3)*, 285-293.
20) Rehder, G.; Kirby, S.H.; Durham, W.B.; Stern, L.; Peltzer, E.T.; Pinkston, J. *MBARI report*. **2001**.
21) Okubo, A. *Deep Sea Res.* **1971**, *18*, 789-802.
22) Socolofsky, S.A..; Adams, E.E. *J. Hydraul. Res.* **2002**, *40(6),* 661-672.

TABLE 1. Summary of field data and calculated results from three injections

Experiment	*163_1107*	*164_1226*	*164_1232*
Observed initial behavior	floating	sinking	neutral
Injection depth (m)	1099	1251	1297
Densities (kg/m^3)			
CO_2 liquid	943	955	957
Seawater	1032.60	1033.31	1033.53
CO_2 hydrate	1100	1100	1100
Overall composite	1032.57	1033.34	1033.53
Average velocities (m/s)	0.06	-0.02	0
Initial volume of composite (x 10^{-6} m^3)	0.687	0.986	0.692
Volumetric flowrate ratio (Q_{CO2}/Q_W)	1	0.2	0.2
CO_2 hydrate conversion (x_h)	0.2862	0.2596	0.2551
Minimum calculated conversion for sinking composite ($x_{h\ min}$)	0.2864	0.2593	0.2551

TABLE 2. Mean sinking depth (rising height) in meters of CO_2 plumes

Hydrate Conversion (%)	Initial Plume Composition	CO_2 Loading in kg/s			
		1	10	100	1000
~25	composite particles	60	110	200	350
100	solid hydrate particles	250	400	700	1200
0	liquid CO_2 droplets	(30)	(30)	(70)	10

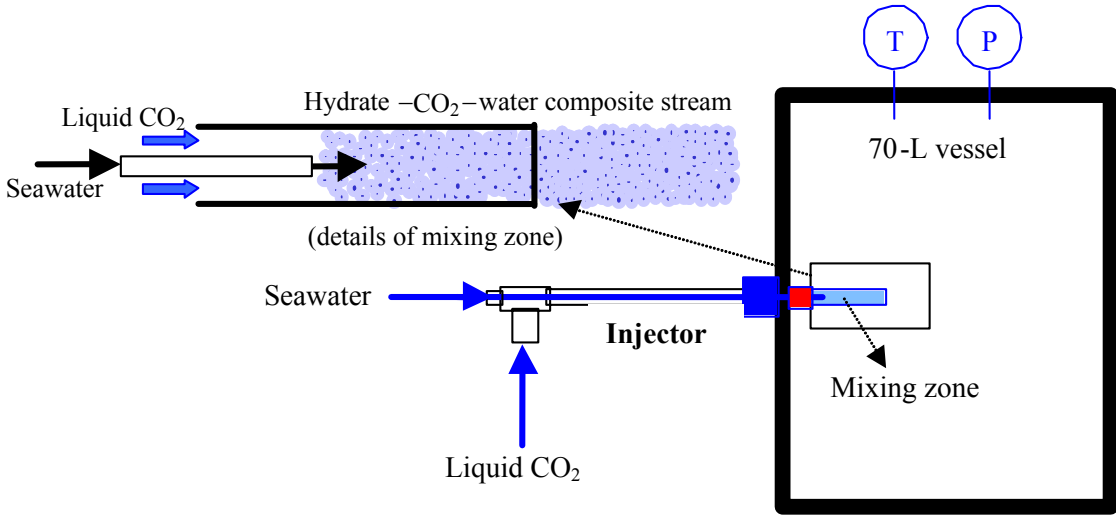

FIGURE 1 Experimental arrangement showing a novel design for a co-flow injector, which produces a high interfacial area between liquid CO_2 and water in a mixing zone before the mixture is injected into the surrounding seawater. Upon exiting the injector, the composite contains CO_2 hydrate and liquid CO_2.

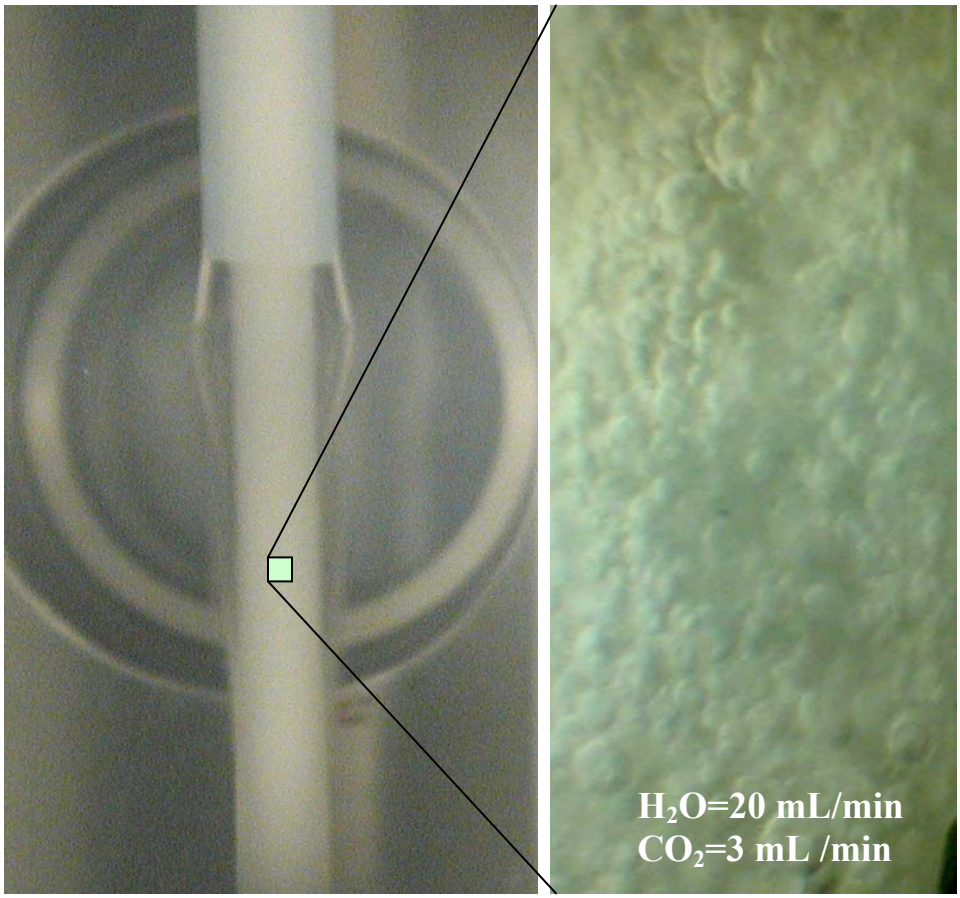

FIGURE 2 The surface of the hydrate composite as observed through a borescope, showing the small hydrate particles fused together.

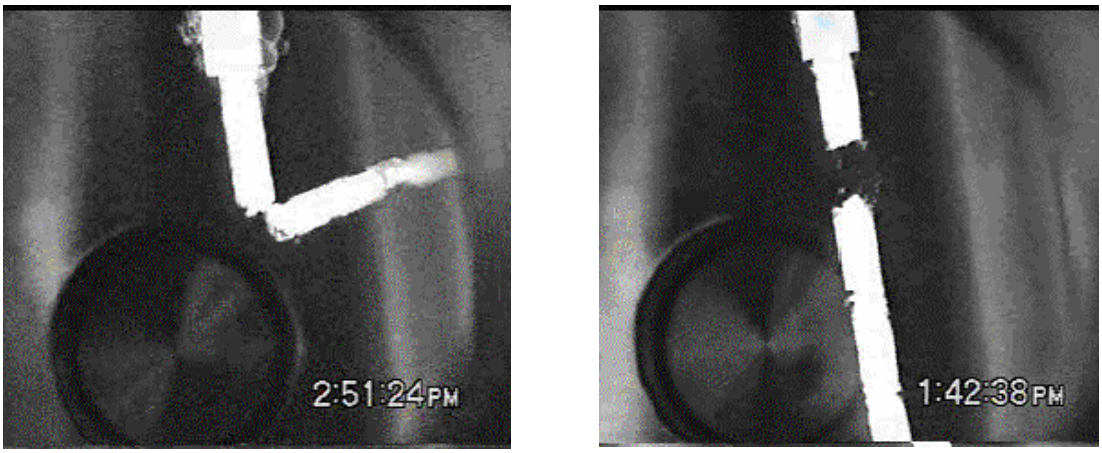

a *b*

FIGURE 3
(a) positively buoyant hydrate composite. P = 10.5 MPa; T = 4.6 °C; flowrates: H_2O = 21 mL min^{-1}, CO_2 = 5 mL min^{-1}
(b) negatively buoyant hydrate composite. P = 13.2 MPa; T = 4.1 °C; flowrates: H_2O = 23 mL min^{-1}, CO_2 = 6 mL min^{-1}

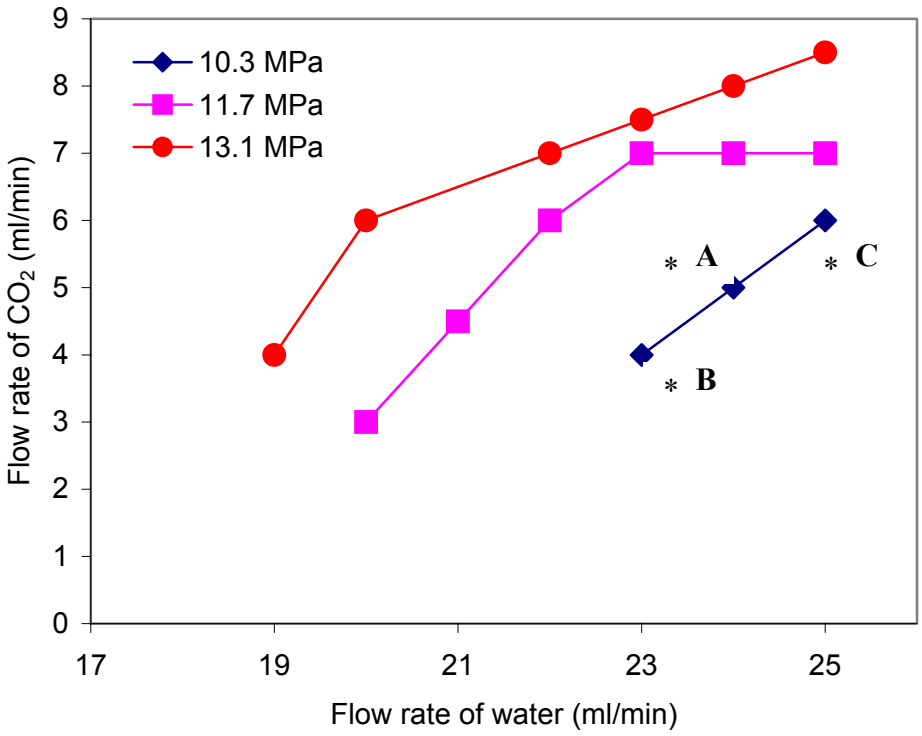

FIGURE 4 Density boundaries for producing a negatively buoyant hydrate composite. Point **A** denotes flow conditions for a positively buoyant hydrate composite at 10.3 MPa. Decreasing the CO_2 flowrate (to reach point **B**) or increasing the water flowrate (to reach point **C**) produces a sinking hydrate composite.

a b

FIGURE 5 (a) The ROV *Ventana* being lowered into Monterey Bay. The Plexiglas injection box is to the left. (b) CO_2 hydrate injection in Monterey Bay, California, using the coflow jet reactor at 1290-m depth (P = 13.1 MPa and T = 3.2 °C). Flowrates for water and CO_2 were 50 and 10 mL/min, respectively. *Note:* The light on one of the particles in the field experiment comes from a Raman spectrometer that was unsuccessfully used to analyze composite particles.

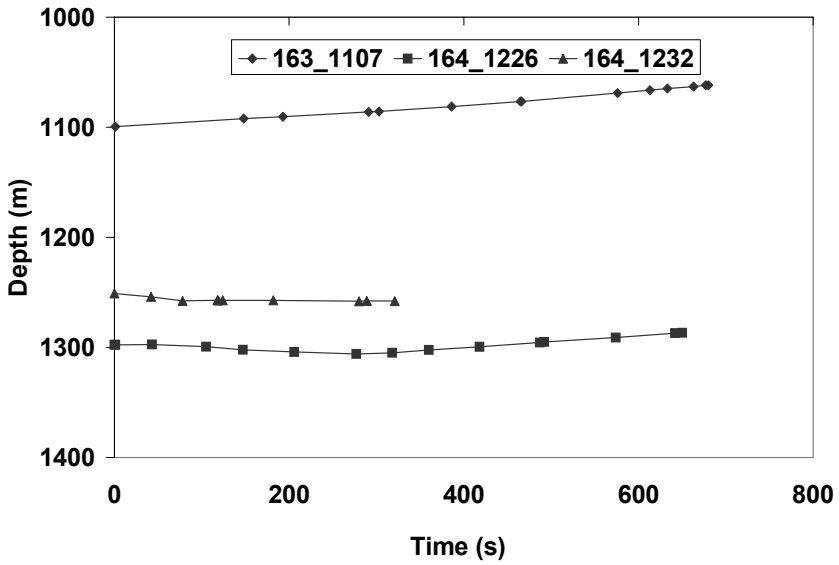

FIGURE 6 Plot of depth versus time, indicating the vertical movement of particles after injection.

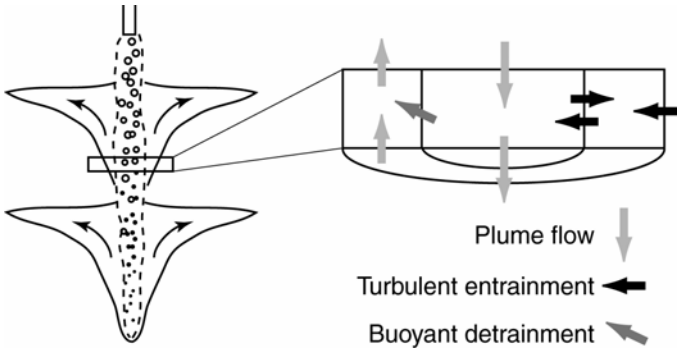

FIGURE 7 Integral model control volume.

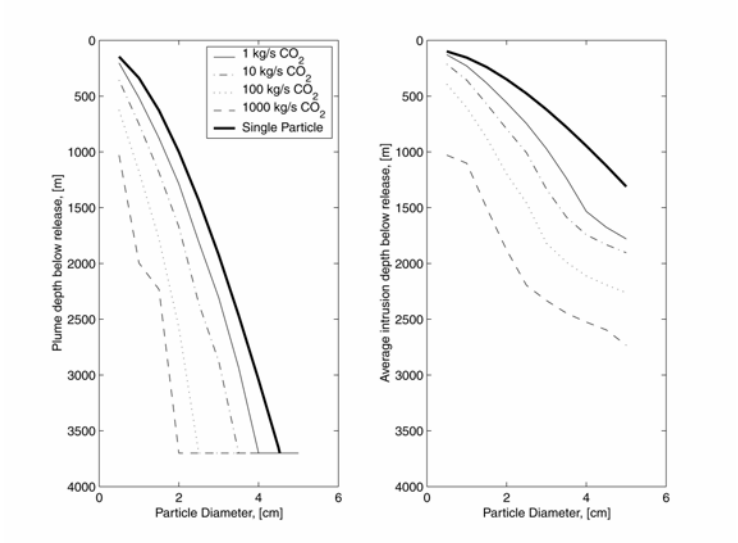

FIGURE 8 Maximum plume and average intrusion depths versus particle diameter for different CO_2 release rates. Dark line refers to falling isolated particles.

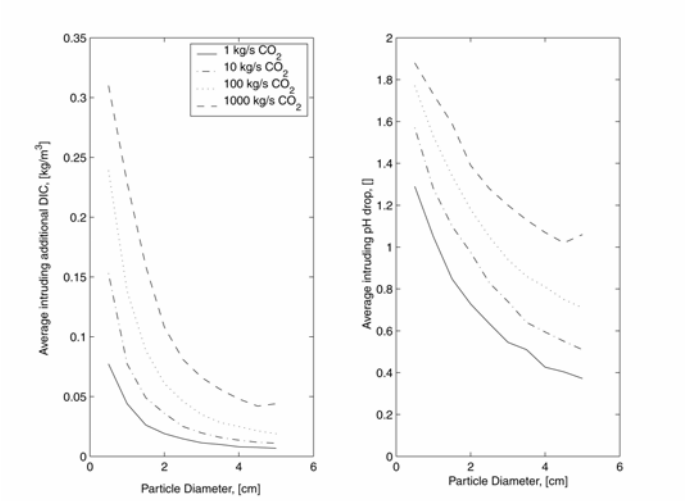

FIGURE 9 Average intrusion changes in DIC and pH versus particle diameter for different CO_2 release rates.

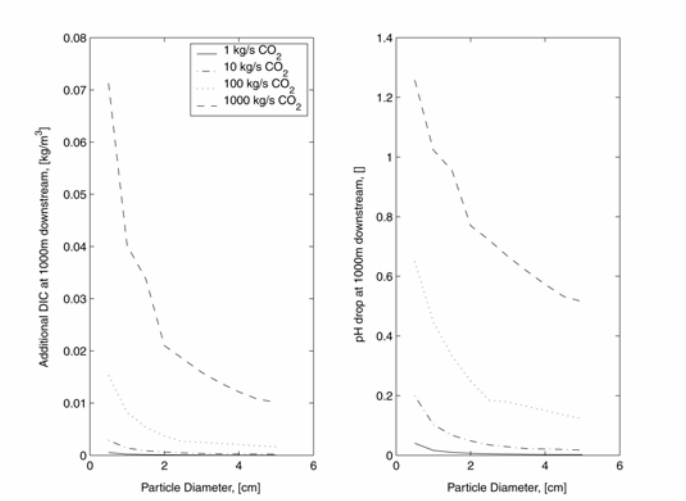

FIGURE 10 Far field (1000 m downstream) change in DIC concentration and pH versus particle diameter for different CO_2 release rates.